Robust Extraction of Frequency-dependent Dielectric Properties from Time Domain Reflectometry

Chih-Ping Lin and Yin Jeh Ngui
Department of Civil Engineering
National Chiao Tung University
Hsinchu, Taiwan
cplin@mail.nctu.edu.tw

***Abstract*—Most dielectric spectroscopy techniques require careful system calibration, tedious measurement, specially designed probes, precise input source and some even involved complicated inversion models. This study presented two robust and model-free signal processing approach to extract frequency-dependent dielectric properties from time domain reflectometry (TDR), namely phase velocity analysis (PVA) and multiple reflection analysis (MRA). PVA determines frequency-dependent apparent dielectric permittivity (ADP) from the top and end reflections in TDR signal. MRA encompasses all multiple reflections of TDR signal to measure the complex dielectric permittivity (CDP) spectrum. This innovative approach involves decomposing the first top reflection and the subsequent multiple reflections from TDR signal, comparing their spectral MRA-ratio and inverting the frequency-dependent CDP from the measured MRA-ratio. Both their reliability were evaluated numerically and experimentally from 10MHz–1GHz. Since they are independent of source function and preceding system mismatches, dielectric spectroscopy can be conveniently conducted in laboratory and field, without complicated system setup and calibration.**

Keywords--TDR, complex dielectric permittivity, dielectric spectroscopy, phase velocity analysis, multiple reflection analysis

I. INTRODUCTION

Dielectric spectroscopy holds a significant role in revealing the materials' electrical properties frequency dependency, including the polarization, relaxation and energy dissipation behaviour of materials at various frequency range [1]. In soil physics, dielectric spectroscopy reveals the macroscopic microwave dielectric behaviour of the soil-water mixtures affected by soil type, moisture content, electrical conductivity and dry density [2], [3].

Current practice of dielectric spectrum measurement mostly require careful system calibration, tedious sample preparation time, precise input source, prior information of system input function and some even require complicated inversion models. Several novel techniques were proposed in complex dielectric permittivity (CDP) measurement to prevent tedious calibrations of all system sections, such as triple-short probe calibration [4], short-open-load calibration [5] and two different probe length method [6]. Specifically designed probes and multiple calibrations were necessary nonetheless. Dielectric spectroscopy in the field is particularly difficult and time-consuming due to complicated system setup and delicate probe design, especially for broadband dielectric spectroscopy at several hundred MHz. In light of all these limitations, demand for a simple yet efficient dielectric spectroscopy technique is rising.

II. THEORETICAL BACKGROUND OF PVA

Lin et al. [7] proposed a simple robust phase velocity analysis (PVA) method to determine frequency-dependent apparent dielectric constant from the top and end reflections in a time domain reflectometry (TDR) signal. PVA calculates the phase shift between the two extracted TDR reflections and computes the apparent dielectric spectrum of material under test (MUT) from the phase velocity.

TDR probe measurement system generally involves a pulse generator, oscilloscope, transmission line, and a sensing probe. A step pulse is sent by the pulse generator into leading cables and electromagnetic (EM) wave is exposed to the MUT along the sensing probe at the end of transmission line. The dominant mode of the recorded TDR signal is essentially 1-D transverse electromagnetic (TEM) mode. The propagation velocity V_{TEM} of the EM wave in material of CDP(ε^*) is

$$V_{TEM} = \mathrm{c}/\sqrt{\frac{\varepsilon'}{2}\left[\sqrt{1+\left(\frac{\varepsilon^{ii}}{\varepsilon'}\right)^2}+1\right]} \tag{1}$$

where c is the speed of light, ε' and ε^{ii} is the real part and the imaginary part of CDP respectively. The system modelling of TDR is modelled using the transmission line theory. The propagation function H describes the wave decay and phase changes during the wave propagation in the transmission line:

$$H(x,\varepsilon^*(f)) = exp[-\gamma(f)x] = \exp[-\alpha(f)x - jk(f)x] \tag{2}$$

where j is $\sqrt{-1}$, x is the traveling distance, α is the attenuation constant, k is the phase constant (wavenumber)

$$\mathrm{k} = \frac{2\pi \mathrm{f}}{\mathrm{c}}\sqrt{\frac{\varepsilon'}{2}\left[\sqrt{1+\left(\frac{\varepsilon^{ii}}{\varepsilon'}\right)^2}+1\right]} = \frac{2\pi \mathrm{f}}{V_{TEM}} \tag{4}$$

Despite wave attenuation and phase change, reflections and transmissions occur at characteristic impedance (Z_c) discontinuous interfaces, which can be described using the reflection coefficient ρ_i and transmission coefficient τ_i

$$\rho_{\mathrm{i}} = \frac{Z_{c,i+1}-Z_{c,i}}{Z_{c,i+1}+Z_{c,i}} \tag{5}$$

$$\tau_{\mathrm{i}} = 1+\rho_i \tag{6}$$

where impedance mismatch lies between section i and $i+1$,

978-1-5386-4593-2/18/$31.00 ©2018 IEEE

Z_c is dependent on both the transmission line geometric impedance (Z_p) and the dielectric permittivity of the material,

$$Z_c = \frac{Z_p}{\sqrt{\varepsilon^*(f)}} \tag{7}$$

Fig. 1 shows the ray tracing diagram of an input X propagating along the cable and all occurring transmitted and reflected ray paths are illustrated for better visualization. Despite the preceding system mismatches, the two major interface discontinuities between cable-probe and the probe end produce the two reflection pulses utilized in PVA analysis. The first reflection at beginning of sensing section (hereinafter referred to as R_1) and the second reflection from the probe end (hereinafter referred to as R_2) can be expressed respectively as

$$R_1 = X \cdot F \cdot \rho_1 \cdot B \tag{8}$$

$$R_2 = X \cdot F \cdot H(2L, \varepsilon^*(f)) \cdot (1 - \rho_1^2) \cdot B \tag{9}$$

where F and B are the forward and backward propagation system function respectively, ρ_1 is the reflection coefficient at Interface I, L is the probe length. X, F, and B are the system parameters and not the targets being measured. The dielectric information $\varepsilon^*(f)$ of interests lies within $H(x, \varepsilon^*(f))$ and ρ_1. There is a simple way to deal with this. Inspecting the phase term of R_2/R_1, the aforementioned system parameters can be cancelled out for non-trivial situations, as shown below

$$\angle(R_2/R_1) = \phi_p - 2kL = \angle\left(\frac{1-\rho_1^2}{\rho_1}\right) - 2kL \tag{10}$$

where $\angle$ is the phase angle operator, the term $2kL$ is the phase shift due to H, ϕ_p is the phase perturbation caused by the ρ and is undetermined without prior knowledge of the MUT's CDP, but ϕ_p is equal to π by considering only the real part of CDP. The imaginary part of CDP would only induce slight difference to ϕ_p from π if compared to $\angle(R_2/R_1)$, which difference is negligible especially at higher frequencies. Since it is common to have a sensing probe with Z_c lower than its leading cable, both ρ_1 and ϕ_p term are hence negative. The phase velocity in MUT can be approximated by

$$V_{PVA} = \frac{4\pi fL}{\pi - \angle(R_2/R_1)} = \frac{4\pi fL}{\angle(-R_1/R_2)} \cong V_{TEM} \tag{11}$$

$\angle(-R_1/R_2)$ is the phase shift between the two reflections and is also denoted as $\Delta\phi$. By extracting the first two main reflections from TDR signals and performing fast Fourier Transform (FFT) on the time-domain signals, the frequency-dependent phase velocity above is measured from the phase difference of the two reflections. The apparent dielectric permittivity (ADP) spectrum, $\varepsilon_a(f)$ is computed directly by

$$\varepsilon_{a(f)} = \frac{c}{V_{PVA}(f)} \tag{12}$$

This is the theoretical basis for the PVA method. Neither system calibration nor inversion are involved during the ADP measurement, which allowed PVA to be highly convenient and computationally efficient. The proposed method can be easily applied in field measurements and provide real-time ADP spectrum directly from measured TDR time domain signals.

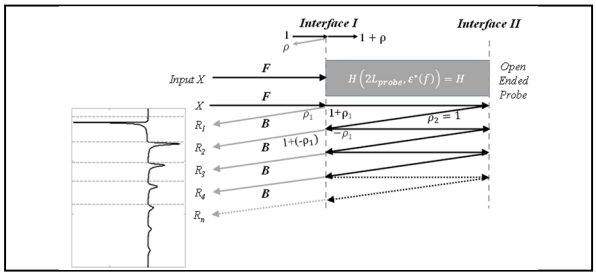

Fig. 1. Ray tracing diagram for all TDR reflections.

III. Theoretical Background of MRA

Multiple reflections in TDR signals are usually neglected during signal processing and analysis, which its importance was underestimated. Previous PVA study [7] discovered that by including the multiple reflections of time-domain signals, ADP spectrum of highly dispersive materials are still measurable with slight deviation from theoretical value. Based on this insight, a multiple reflection analysis (MRA) is proposed by Lin et al. [8], which considers all the multiple reflections from the sensing probe section, and aimed at measuring complete CDP spectrum at broader frequency range within 10MHz–1GHz. The key to this approach is to decompose TDR signal into the first top reflection and the remaining all multiple reflections. Spectral ratio of these two parts (MRA ratio) was theoretically derived as a function of CDP. CDP can be uniquely inverted from the measured MRA ratio ($\mathrm{MRA_{mea}}$). Neither prior information regarding input signal nor dielectric permittivity model is required in the analysis. Having both the simplicity of PVA and the capability of CDP measurement, MRA is computationally efficient and only requires simple system calibration, making it especially suitable for field applications.

MRA takes the spectral ratio of the remaining reflections after R_1 ($R_{remaining}$, i.e. $R_2 + R_3 + R_4 + \cdots$) to R_1. $R_{remaining}$ can be derived as

$$R_{remaining} = X \cdot F \cdot B \cdot H \cdot (1 - \rho_1^2) \cdot \sum_{k=2}^{\infty} [H \cdot (-\rho_1)]^{(k-2)} \tag{13}$$

where H is the abbreviated sensing section system function of $H(2L, \varepsilon^*(f))$. Replacing $\mathrm{k = n + 2}$, the last term is a geometric series summation and $R_{remaining}$ can be rearranged as

$$R_{remaining} = X \cdot F \cdot B \cdot H \cdot (1 - \rho_1^2) \cdot \frac{1}{1+\rho_1 H} \tag{14}$$

By comparing R_1 in (8), MRA ratio is now

$$MRA = \frac{R_{remaining}}{R_1} = \frac{H \cdot (1-\rho_1^2)}{\rho_1 \cdot (1+\rho_1 H)} \tag{15}$$

where $|-\rho_1 H| < 1$ and $\rho_1 \neq 0$ must be satisfied for MRA to be valid and non-trivial. Equation (15) shows that the system functions X, F, B are cancelled out and MRA ratio is purely a function of H and ρ_1, where the CDP of interests lies. This shows that this method is independent of input function and leading transmission line sections.

A typical TDR waveform measured by a matched probe in water is shown in Fig. 2(a) to illustrate MRA measurement procedures. TDR step pulse signal is first differentiated into impulse signal (Fig.2(b)) and next decomposed into $r_{remaining}$

(Fig. 2(c)) and r_1 (Fig. 2(d)), before performing FFT on the time-domain signals. $\mathrm{MRA_{mea}}$ are computed by comparing their spectral ratios. Two system parameters Z_{ch}/Z_{p1}, L are provided to generate H, ρ_1 and theoretical MRA (MRA_{theo}) in (15), where Z_{ch}/Z_{p1} is required for ρ_1

$$\rho_1 = \frac{Z_{c1}-Z_{ch}}{Z_{c1}+Z_{ch}} = \frac{1-\frac{Z_{ch}}{Z_{c1}}}{1+\frac{Z_{ch}}{Z_{c1}}} = \frac{1-\frac{Z_{ch}}{Z_{p1}}\sqrt{\varepsilon_1^*}}{1+\frac{Z_{ch}}{Z_{p1}}\sqrt{\varepsilon_1^*}} \tag{16}$$

where Z_{ch} and Z_{c1} are the characteristic impedances of probe head and probe sensing section respectively, Z_{p1} is the geometric impedance of the probe sensing section. An arbitrary yet reasonable initial guess consisting both real and imaginary parts of CDP is selected for MRA fitting optimization. $\mathrm{MRA_{theo}}$ are computed based on the opted guess, starting from the lowest frequency. $\mathrm{MRA_{theo}}$ is optimized with regard to $\mathrm{MRA_{mea}}$ until the minimum cost is found for the CDP cost function (root-mean-square error between $\mathrm{MRA_{theo}}$ and $\mathrm{MRA_{mea}}$). This optimization process is iterated by every frequency steps within 10MHz–1GHz until the complete CDP spectrum is generated.

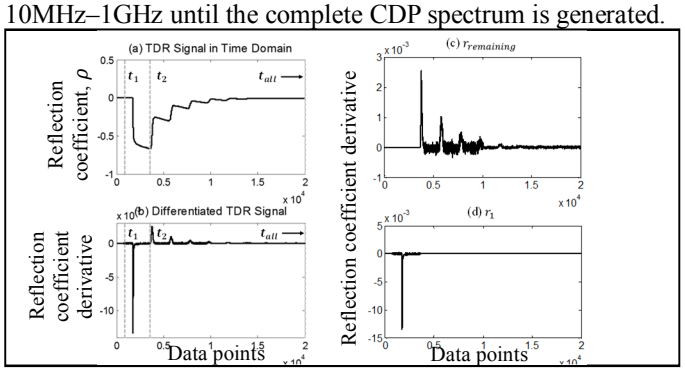

Fig. 2. MRA signal processing (tap water as example): (a) TDR step signal. (b) Differentiated impulse signal. (c) Extracted $r_{remaining}$. (d) Extracted r_1.

IV. Evaluation in Simulated Signals

Both PVA and MRA is evaluated with synthetic TDR data and experimental data. Measurement system is comprised of a three-section transmission line model, including a 10m 50Ω coaxial cable, a 0.1m 50Ω matched probe head and a 0.17m coaxial probe sensing section with $Z_p = 95\,\Omega$. Three MUTs with different dielectric dispersion and electrical conductivity characteristics were simulated, namely distilled water, acetone, and ethanol [7]. Synthetic TDR signal is simulated using a comprehensive wave propagation model by Lin and Tang [9]. Cole-Cole function is selected as the dielectric relaxation model to describe theoretical dielectric behaviours of MUTs. Simulated waveforms are shown in Fig. 3.

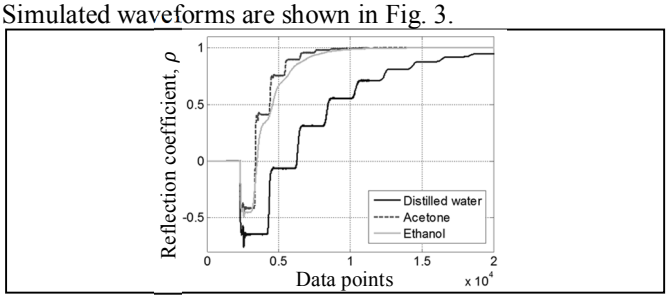

Fig. 3. Synthetic TDR signal of MUTs.

The measured ADP spectrum by PVA and CDP spectrum by MRA is shown in Fig. 4. Reliability of MRA approach is proven numerically. The proposed method is capable of measuring both real and imaginary parts of CDP spectrum with simple system parameter calibration of Z_{ch}/Z_{p1} and L.

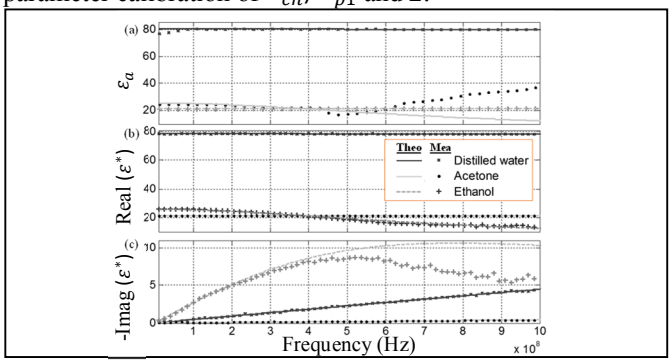

Fig. 4. (a) ADP spectrum from PVA. (b)(c) Real and imaginary part of CDP spectrum from MRA.

V. Conclusions

PVA and MRA approaches presented in this study are rapid, robust, model-free, source function independent in ADP/CDP spectrum measurement within TDR frequency range of 10MHz-1GHz by using time-domain signals. Straightforward algorithm of these two approaches enables dielectric spectroscopy to be conveniently conducted in both laboratory and field, without complicated system setup and calibration. This allow in-situ ADP/CDP spectrum monitoring to be performed reliably and economically, which may possibly be a breakthrough in the dielectric spectroscopy field.

References

[1] U. Kaatze, "Measuring the dielectric properties of materials. Ninety-year development from low-frequency techniques to broadband spectroscopy and high-frequency imaging," Meas. Sci. Technol., vol. 24, no. 1, p. 012005, January 2013.

[2] T. J. Heimovaara, "Frequency domain analysis of time domain reflectometry waveforms: 1. Measurement of the complex dielectric permittivity of soils," Water Resour. Res., vol. 30, no. 2, pp. 189–199, February 1994.

[3] C.-P. Lin, "Frequency domain versus travel time analyses of TDR waveforms for soil moisture measurements," Soil Sci. Soc. Am. J., vol. 67, no. 3, pp. 720–729, 2003.

[4] E. Piuzzi, A. Cataldo, G. Cannazza, and E. De Benedetto, "An Improved Reflectometric Method for Soil Moisture Measurement Exploiting an Innovative Triple-Short Calibration," IEEE Trans. Instrum. Meas., vol. 59, no. 10, pp. 2747–2754, October 2010.

[5] C.-P. Lin, S.-H. Tang, C.-H. Lin, and C.-C. Chung, "An improved modeling of TDR signal propagation for measuring complex dielectric permittivity," J. Earth Sci., vol. 26, no. 6, pp. 827–834, 2015.

[6] A. Szyplowska, A. Wilczek, M. Kafarski, and W. Skierucha, "Soil Complex Dielectric Permittivity Spectra Determination Using Electrical Signal Reflections in Probes of Various Lengths," Vadose Zone J., vol. 15, no. 3, 2016.

[7] C.-P. Lin, Y. J. Ngui, and C.-H. Lin, "A novel TDR signal processing technique for measuring apparent dielectric spectrum," Meas. Sci. Technol., vol. 28, no. 1, p. 015501, 2017.

[8] C.-P. Lin, Y. J. Ngui, and C.-H. Lin, "Multiple Reflection Analysis of TDR Signal for Complex Dielectric Spectroscopy," IEEE Transactions on Instrumentation and Measurement, pp. 1–13, 2018.

[9] C.-P. Lin and S.-H. Tang, "Comprehensive wave propagation model to improve TDR interpretations for geotechnical applications," *Geotech. Test. J.*, vol. 30, no. 2, pp. 90–97, 2007.